Y_2SiO_5 coatings fabricated by RF Magnetron Sputtering

Surface and Coatings Technology Vol. 273 (2013) pages 88–94
http://dx.doi.org/DOI: 10.1016/j.surfcoat.2013.08.015.

Y_2SiO_5 coatings fabricated by RF Magnetron Sputtering

Peter Mechnich[1], Annika Lange, Reinhold Braun, Claudia Büttner[2]

German Aerospace Center (DLR), Institute of Materials Research

Address: Linder Höhe, 51170 Cologne, Germany

[1] corresponding author; e-mail: peter.mechnich@dlr.de

Phone +49-2203-601-2100; Fax +49-2203-696480;

[2]now: MTU Aeroengines, Munich, Germany

Abstract

Yttrium monosilicate (Y_2SiO_5) is considered a promising material for environmental barrier coatings (EBC) for ceramic matrix composites (CMC). Y_2SiO_5 coatings were deposited on all-oxide and non-oxide CMC by magnetron sputtering, respectively. As deposited Y_2SiO_5 is X-ray amorphous, homogenous, and virtually free of cracks and macropores. Annealing performed between 1273 and 1473 K induces crystallization of metastable X_1-Y_2SiO_5, apatite-type $Y_{4.67}(SiO_4)_3O$ and finally stable X_2-Y_2SiO_5. Annealing also produces significant pore coalescence and re-crystallization. Experiments performed with Al_2O_3-based CMC prove the fundamental instability of the Y_2SiO_5/Al_2O_3 interface at high temperatures, however no detrimental melting is observed and a well-bound $Y_2Si_2O_7$/YAG double layer is developing. Experiments with CVD-SiC coated C/SiC CMC in different atmospheres revealed that SiC oxidation to SiO_2 favors adhesion of Y_2SiO_5 coatings. The SiO_2 layer on top of SiC reacts with Y_2SiO_5 to highly porous $Y_2Si_2O_7$ which is able to bridge gaps at the Y_2SiO_5/SiC interface. However, the thin SiO_2 interphase may be critical with respect to thermal cycling. As a preliminary conclusion, sputtered Y_2SiO_5 coatings are considered more advantageous for all-oxide CMC.

Keywords: Y_2SiO_5; magnetron sputtering; coatings; ceramic matrix composites

1. Introduction

The application of ceramic matrix composites (CMC) in combustion environments of gas turbines, such as combustor liners or nozzle guide vanes, requires long-term thermochemical stability. State of the art non-oxide CMCs consist of carbon or SiC fibers embedded in SiC matrices. Frequently an additional SiC overlay fabricated by pack-cementation or chemical vapor deposition (CVD) is employed as oxidation protection. State-of-the-art oxide/oxide CMCs consist of mullite or alumina fibers embedded in submicron mullite or alumina matrices. At high service temperatures and under attack of rapidly flowing, water-vapor rich combustion gases SiC, mullite and alumina are prone to recession due to formation of volatile hydroxide species such as $Si(OH)_4$ and $Al(OH)_3$. The application of environmental barrier coatings (EBC) is considered a solution for the degradation problem: EBCs promise higher corrosion resistance and therefore increased service lifetime and temperature capability of components. Thermodynamic compatibility and low thermal mismatch of EBC and CMC materials are required with respect to high service temperature under thermocyclic load.

In recent years, yttrium oxosilicate Y_2SiO_5 gained attention as potential material for oxidation protection of carbon-based CMC [1-3] as well as EBC for silicon-based CMC [4]. In combustor rig experiments polycrystalline Y_2SiO_5 ceramics exhibited water-vapor recession rates of two to three orders of magnitude lower than SiC, mullite or alumina [5,6]. Previously published values for the coefficients of thermal expansion (CTE) of Y_2SiO_5 are scattering significantly [7-10]. Whereas CTE values of around 5-6 ppm were found in high-temperature XRD [8] a CTE of about 8.4 ppm/K was found for single-phase Y_2SiO_5 compacts by dilatometry [11]. Such conflicting

results have been attributed to presence of even small amounts of impurities like $Y_2Si_2O_7$ [11]. Despite of these inconsistencies CTE of Y_2SiO_5 fits well to that of state-of-the-art CMC materials such as SiC, mullite or alumina, hence CTE mismatch negatively affecting coating durability is considered low. Moreover, the low oxygen permeability and diffusivity of Y_2SiO_5 is considered favorable for EBC functionality [12,13]

Yttrium-silicate coatings have been manufactured by a variety of deposition techniques. However, coatings based upon mixtures of Y_2SiO_5 and $Y_2Si_2O_7$ have been employed rather than pure Y_2SiO_5 coatings. This composite-coating concept aims at a better CTE adaption to SiC-based substrates. Fabrication methods reported in literature include slurry dip-coating and reaction sintering [1,2], low pressure plasma spraying [3], air plasma spraying [14], electrophoretic deposition [15,16] and dip-coating and sintering of Y_2O_3-filled polysiloxanes [17]. Stoichiometric Y_2SiO_5 coatings were fabricated by APS [8] and laser-CVD [18,19]. Y_2SiO_5 coatings are frequently amorphous in the as deposited state. Crystallization of metastable species such as the low-temperature X_1-Y_2SiO_5 polymorph or the apatite-type Y-silicate $Y_{4.67}(SiO_4)_3O$ A is commonly observed upon annealing. Plasma-sprayed Y_2SiO_5 exhibits irreversible expansion upon first annealing at 1473 K explained by crystallization of X_1-Y_2SiO_5, stabilization of the desired high-temperature X_2-Y_2SiO_5 polymorph requires annealing above 1473 K [8]. Y_2SiO_5 coatings fabricated by laser-CVD exhibit a complex crystallization behavior being sensitive to deposition temperature and pressure. Beside the Y_2SiO_5 polymorphs apatite-type $Y_{4.67}(SiO_4)_3O$ and δ-$Y_2Si_2O_7$ were observed as crystalline species at deposition temperatures beyond 1200 K [18]. The present work reports on the microstructural development of

all-oxide and non-oxide CMC with magnetron-sputtered stoichiometric Y_2SiO_5 coatings with special focus on phase formation and microstructural evolution.

A preliminary assessment of the suitability of such coatings as EBC for CMC is given.

2. Experimental Procedure

Y_2SiO_5 coatings were deposited on DLRs standard standard all-oxide and non-oxide ceramic oxide ceramic matrix composites (CMC). The filament wound all-oxide CMC consists of mullite/Al_2O_3 fibers embedded in a porous Al_2O_3 matrix. The non-oxide CMC consists of C-fibers embedded in a SiC matrix and is coated with a CVD SiC outer layer. Coatings were fabricated using a batch-type magnetron sputtering facility (Z 400, Systec SVS vacuum coatings, Karlstadt, Germany). A dense polycrystalline Y_2SiO_5 disk with a diameter of 100 mm was employed as target. HF-sputtering was performed at a target power of 400 W at a total pressure of $5x10^{-6}$ bar in Ar (28 sccm); sputter times typically were 8 hours. The substrate temperature during the deposition process was approximately 400 K. Heat treatments of coated specimen were carried out in a resistor-heated tube furnace (RHTC 80-450/15, Nabertherm, Lilienthal, Germany). Coated CMC samples were heated in variable quasi-static atmospheres (air, N_2, CO/N_2) with 10 K/min to temperatures between 1273 and 1673 K and isothermally annealed for 1 hour, respectively.

Phase analyses were performed using X-ray powder diffraction (XRD) (Siemens D 5000, Cu-Kα radiation and secondary graphite monochromator, EVA/Topas 4.2 software package, Bruker AXS, Karlsruhe, Germany). Microstructural analyses were carried out using scanning electron microscopy (SEM) (DSM Ultra 55, Carl Zeiss NTS, Wetzlar, Germany) equipped with an energy dispersive X-ray spectroscopy (EDS) system (Inca, Oxford Instruments, Abingdon, UK).

3. Results and Discussion

3.1 Y_2SiO_5 coatings for all-oxide CMC

The deposition of Y_2SiO_5 under the chosen sputtering conditions is slow: After 8 hours, coating thicknesses in a range of 15-20 μm were observed**,** i.e. a deposition rate in the range of 2 μm/h. Figure 1 features top view (left hand) as well as a cross-sectional view of a coating deposited on a Al_2O_3/Al_2O_3 CMC substrate. The surface is quasi crack-free and is exhibiting a cauliflower-like morphology. The overall appearance is vitreous, i.e. no grains are visible. XRD analysis confirmed the as-deposited coatings are amorphous. The cross section reveals that, despite of their glassy nature, the coatings exhibit some kind of textured morphology. Approximately 25° tilted columnar features (clearly distinguishable by contrast variation) are growing out of an approximately 2 μm thick root zone exhibiting also some intercolumnar porosity. In order to validate the accuracy and homogeneity of the sputter process, an EDS scan was performed across the as-deposited, X-ray amorphous Y_2SiO_5 coating. EDS quantification gave no evidence for O_2-deficiency. In figure 2 the normalized cation content (mol%) is plotted for 50 individual EDS spots. The coating stoichiometry is close to the theoretical value of Y_2SiO_5 (66.6 mol-% Y; 33.3 mol-% Si). Moreover, the favorable through-thickness homogeneity indicates that preferential sputtering of chemical species obviously is not an issue for the chosen experimental conditions. An incubation period in advance of stable growth conditions may explain the formation of the root zone.

Crystallization of ab initio amorphous Y_2SiO_5 coatings was studied by XRD for specimen annealed at 1273, 1373, and 1474 K for one hour in air, respectively. The XRD profile of the 1273 K sample reveals co-existing oxyapatite-type $Y_{4.67}(SiO_4)_3O$ and X_1-Y_2SiO_5 (fig. 3, lower profile). Moreover, XRD gives evidence for textured

crystallization of the oxyapatite phase: Peak intensity ratios of $Y_{4.67}(SiO_4)_3O$ listed in the ICDD-PDF database (card #30-1457) return (211) at approximately 32° 2-θ as strongest XRD reflection. In the present case much higher than expected peak intensities are observed for the (200), (102), and (400) reflections at 26.5°, 28.7° and 54.5° 2-θ, respectively. The 1373 K sample exhibits a complex XRD pattern with multiple peak overlap, however beside $Y_{4.67}(SiO_4)_3O$ and X_1-Y_2SiO_5 newly formed X_2-Y_2SiO_5 is evident. A distinct evolution has occurred in the 1473 K sample, where all XRD reflections can be assigned unambiguously to the high-temperature X_2-Y_2SiO_5 polymorph. Note that all XRD profiles include three weak corundum peaks (C) originating from the Al_2O_3-substrate.

The microstructures of annealed coatings, including top-views and cross sections were analyzed by SEM, respectively. The top view of the 1273 K sample reveals that nanoscaled crystals have formed at the cauliflower-type surface (fig. 4). The cross-section clearly reveals that the seemingly columnar microstructure of the as-deposited state now appears as textured arrangement of elongated grains which are separated by aligned pores. Evidently these grain boundaries appear as dark contrasted, aligned features in the SEM top-view. Taking into account the preferred crystallographic orientation observed in XRD, it is concluded that large, mostly elongated grains represent the major Y-oxyapatite phase, whereas the nanoscaled crystals may rather be assigned to X_1-Y_2SiO_5. A fundamentally different morphology is found in the root zone, where isometric, seemingly untextured oxyapatite grains are dominating.

The 1373 K sample (fig. 5) exhibits significant larger crystals at the surface. The size distribution is broad, grain sizes typically range from 0.1 to 0.5 μm. Features originating from aligned pores, as observed in the 1273 K sample, are not evident.

At first glance, there seems to be no substantial evolution of the microstructure in the cross-section. However, although pore sizes seem unchanged, pore alignment is less pronounced. Moreover, the decomposition of elongated Y-oxyapatite apparently produces smaller, isometric crystals, presumably X_2-Y_2SiO_5.

As could be anticipated from XRD results, a considerable microstructural evolution is observed in the 1473 K sample (fig. 6). The coating surface now seems to be almost dense and consists of much larger crystals typically having grain sizes in the 0.5 to 2 μm range. The cross-section reveals that there is still some pore alignment but grain orientation has quasi disappeared. The microstructure now is looking much denser, consisting of isometric, approximately 1-2 μm X_2-Y_2SiO_5 grains. Pores have coalesced but still are located predominantly at grain boundaries. Pore coalescence is most pronounced in the topmost coating segment and in the root zone, respectively. The overall appearance suggests that the coating is quasi dense, i.e. has only closed porosity and consequently should be gas-tight. However, it must be emphasized that cracks extending through the coatings thickness are observed occasionally. These cracks are presumably no preparation artifacts; therefore achieving a complete sealing of the substrate seems uncertain.

The 1573 K sample is characterized by progressively dissipating small Y_2SiO_5 grains, whereas the maximum Y_2SiO_5 grain size is still in the 2 μm range (fig. 7). This behavior is easily explained by surface energy minimization of the chemically closed system (“Ostwald ripening”). The coating cross-section reveals the coinciding coalescence of pores. Similar to the 1473 K sample cracks are observed occasionally at the coating surface as well as in the bulk. The root zone does not exhibit a distinguished microstructure, i.e. size and shape of pores and grains are similar to those of the major coating volume. At the coating/substrate interface, however, there

exists a newly formed thin, brightly contrasted zone (see white arrows). The inset in figure 7 discloses that this interface zone features two differently contrasted, approximately 200 nm thick layers. The brighter contrasted layer is located at the boundary to the Al_2O_3 substrate whereas the darker contrasted layer is located adjacent to the Y_2SiO_5 coating. Both layers are obviously due to a chemical reaction between X_2-Y_2SiO_5 and Al_2O_3. Since 1573 K is far below the lowest eutectic temperature of the Y_2O_3-Al_2O_3-SiO_2 system (approximately 1643 K), a solid-state reaction is evident.

Upon annealing at 1673 K, additional ripening of X_2-Y_2SiO_5 grains and progressive coalescence of globular, closed pores in the Y_2SiO_5 layer are obvious (fig. 8). Pore dimensions are now suitable for analysis: on the basis of a binary image a pore volume of approximately 25 % is estimated. Phase transformations are presumably not contributing to pore formation since the Y-silicate phases have similar densities (Y-oxyapatite ~4.6 g/cm^3, X_1-Y_2SiO_5 ~4.8 g/cm^3, X_2-Y_2SiO_5 ~4.5 g/cm^3; calculated from structure data). It can therefore be concluded that the (nano)porosity of as-sputtered coatings has a similar magnitude.

The main feature of the 1673 K sample is the now approximately 5 μm thick reaction zone extending quasi continuously across the Y_2SiO_5 / Al_2O_3 interface. Although the lowest eutectic temperature has been exceeded, the reaction zone appears crystalline and there is no evidence for the formation of an intermediate, partial melt. In order to identify the present phases, an EDS line scan across the reaction zone was performed as indicated by the dotted arrow. In figure 9 the normalized cation content (mol-%) is plotted for each of the 50 individual spots. EDS data unambiguously reveals that the reaction zone between Y_2SiO_5 and Al_2O_3-based CMC is featuring an yttrium-silicate/yttrium-aluminate double layer. The phase co-existing

with X_2-Y_2SiO_5 is obviously the yttrium di-silicate $Y_2Si_2O_7$ which may exhibit some dissolution of Al, in particular in direction of the Al_2O_3-based CMC. The yttrium-aluminate phase exhibits a significant chemical gradient with increasing Al-content in direction to the CMC boundary: at the $Y_2Si_2O_7$ boundary the Al/Y ratio is close to one and is increasing to more than 1.5 adjacent to Al_2O_3. The former stoichiometry would match $YAlO_3$ (Y/Al=1), the latter is approximating $Y_3Al_5O_{12}$ (stoichiometric YAG, Y/Al=1.67). Since the microstructure provides no evidence for a internal phase boundary, it is evident that the entire Y-aluminate layer consists of a YAG-type solid solution. Indeed, metastable YAG off-stoichiometry to a Y-rich composition has been reported previously [20,21]. In analogy it is concluded that the first Y_2SiO_5/Al_2O_3 reaction product is a Y-rich YAG solid solution having $Y_2O_3 \bullet Al_2O_3$ composition and the formation of stoichiometric YAG is occurring by continuous diffusion out of the substrate in later reaction stages. Following this concept, the YAG reaction sequence can be given as

$$(1)\ 2\ Y_2SiO_5 + Al_2O_3 \rightarrow Y_2Si_2O_7 + Y_2O_3 \bullet Al_2O_3$$

$$(2)\ 1.5\ Y_2O_3 \bullet Al_2O_3 + Al_2O_3 \rightarrow Y_3Al_5O_{12}$$

Taking into account the metastability of Y-rich YAG, the bulk reaction can thus be given as

$$6\ Y_2SiO_5 + 5\ Al_2O_3 \rightarrow 3\ Y_2Si_2O_7 + 2\ Y_3Al_5O_{12}$$

From the densities of constituents (X_2-Y_2SiO_5 ~4.5 g/cm^3; α-Al_2O_3 ~4.0 g/cm^3; $Y_2Si_2O_7$ ~4.1 g/cm^3; YAG ~4.5 g/cm^3), a volume balance for the above reaction can be approximated: ~25 vol% X_2-Y_2SiO_5 and ~75 vol% α-Al_2O_3 react to ~50 vol% $Y_2Si_2O_7$ and ~50 vol% YAG, obviously matching well the dimension of the double layer.

The reaction between Y_2SiO_5 and Al_2O_3 can be interpreted in the light of subsolidus thermodynamic data of the Y_2O_3-Al_2O_3-SiO_2 system [22,23]: figure 10 shows an adapted ternary phase diagram showing phase relations calculated for 1673 K [23]. An equimolar composition of Y_2SiO_5 + Al_2O_3 = Y_2O_3•Al_2O_3•SiO_2, i.e. equivalent to 33.3 mol% of each oxide species is considered a plausible and simple model for the Y_2SiO_5 / Al_2O_3 interface in early reaction stages (see dot marker in fig. 10). Evidently, this representative composition is located relatively close to the join between $Y_2Si_2O_7$ and $Y_3Al_5O_{12}$ (see highlighted line in fig. 10) indicating co-existence of these phases. Moreover, the subsolidus phase diagram indicates that Y_2SiO_5 and Al_2O_3 do not co-exist at 1673 K, which unambiguously meets the microstructural observations. The situation in later reaction stages can simply be illustrated by co-existing Y_2SiO_5-$Y_2Si_2O_7$-$Y_3Al_5O_{12}$ and $Y_2Si_2O_7$-$Y_3Al_5O_{12}$-Al_2O_3 where both fields are separated by the $Y_2Si_2O_7$-$Y_3Al_5O_{12}$ join. Since the Al_2O_3 substrate can be regarded as being “infinite” with respect to the Y_2SiO_5 coating, however, thermodynamics will eventually lead to complete decomposition of Y_2SiO_5 to $Y_2Si_2O_7$ and YAG. If temperature and associated diffusion velocity is high enough, this may take place on the long term. It must be emphasized, however, that peak interface temperatures of EBC-coated porous Al_2O_3/Al_2O_3 CMC presumably will be limited to the 1473 K range, and long-term operation temperatures presumably will be significantly lower. Consequently, even if thermodynamically favored, Y_2SiO_5 decomposition will be slow enough to provide an adequate lifetime. As an alternative, the results also suggest that a thin Y-aluminate interlayer (e.g. $Y_3Al_5O_{12}$, $YAlO_3$, or $Y_4Al_2O_9$) could act as a diffusion barrier, decelerating or inhibiting Y_2SiO_5 decomposition. In general the results and literature data on favorable mechanical properties (low modulus, hardness) [24] suggest that it is possible to obtain durable Y_2SiO_5 coatings on Al_2O_3-based substrates which may be employed at temperatures of 1473 K and beyond.

3.2 Y_2SiO_5 coatings for non-oxide CMC

Figure 11 shows the top view as well as a cross-sectional view of a coating deposited on a CVD-SiC coated C/SiC substrate. The cross section reveals that as-deposited coatings exhibit good conformity. In contrast to the as-deposited coating on the oxide substrate the majority of the coating exhibits a vitreous rather than a columnar microstructure. However, also in this case the approximately 2 μm thick root zone with some intercolumnar porosity is indicative for columnar growth. Also in this case the surface is quasi crack-free but the morphology is different to that observed for the oxide substrate (see also fig. 1): The cauliflower features are now more asymmetric which may be related to the higher substrate surface irregularities: CVD-SiC is typically characterized by free growth of sharp-edged pyramidal crystals with broad grain size distribution, therefore uniform deposition is not easily achieved.

Fig. 12 shows the temperature-dependent behavior of the Y_2SiO_5 coated SiC samples upon annealing in N_2 at 1273, 1373, and 1473 K, respectively. The 1273 K sample (fig 12, lower SE image) immediately reveals the weak chemical bonding between oxide coating and non-oxide substrate. A distinct gap between Y_2SiO_5 and pyramidal SiC occurs predominantly in the right-hand region of the interface. However, also the residual interface exhibits a small, but significant gap. Vertical and horizontal cracks are running through the coating. The weak Y_2SiO_5/SiC bonding becomes prevalent at 1373 K, where Y_2SiO_5 is completely detached from the pyramidal CVD-SiC surface (fig. 12, middle SE-image). The scenario changes upon annealing at 1473 K (fig. 12, upper part) where the Y_2SiO_5 coating is not entirely detaching. Instead a newly formed, approximately 1-2 μm thick, porous phase partially fills the gap between coating and substrate. A close-up of the respective Y_2SiO_5/SiC interface is depicted in fig. 13. The EDS analysis revealed that porous

$Y_2Si_2O_7$ has formed at the interface, obviously at the expense of Y_2SiO_5 and amorphous SiO_2 originating from SiC oxidation. Indeed, small droplets of SiO_2 are still wetting SiC. Although annealing was performed in N_2, there was obviously sufficient oxygen in-diffusion, presumably through the Al_2O_3 tube furnace wall, in order to produce the SiO_2 required for Y_2SiO_7 formation. Since the $Y_2Si_2O_7$ interlayer is seemingly beneficial for Y_2SiO_5 adhesion it was obvious to intentionally produce reactive SiO_2 which could act as a chemical “adhesive”. The corresponding annealing experiment was performed at 1473 K in static air (fig. 14). At a glance, the interface now exhibits a quasi-continuous layer of porous $Y_2Si_2O_7$, but also the thin SiO_2 overlay seems to wet the entire SiC surface. The overall coating adhesion seems to be much better than observed upon annealing in N_2, confirming the concept of a SiO_2-enhanced chemical bonding. Conversely, this observation implies that suppressing the SiO_2 formation would result in a very weak bonding of Y_2SiO_5. In order to validate this assumption, a sample was annealed at 1473 K under reducing conditions. This set-up was achieved by co-heating of the sample and carbon felt in the air-filled tube furnace allowing pressure compensation. Assuming ideal gases and complete reaction of O_2 ($C + O_2 \rightarrow 2\ CO$), an estimate of 34 vol% CO results for the N_2/CO furnace atmosphere. The outcome of this experiment is depicted in fig. 15. The Y_2SiO_5 coating is strongly warped or blistered and exhibits massive de-bonding (upper SE-image). Massive degradation effects inside of the Y_2SiO_5 coating become evident at higher magnification. Only the inner part seems to be unaffected Y_2SiO_5 exhibiting small globular porosity. Towards the coatings’ outside there are massive microstructural effects. First, a zone with strong pore coalescence but similar contrast is found in contact with Y_2SiO_5. Then a slightly darker contrasted zone with less porosity is following. Both zones do not show pronounced grain boundaries or faceting. Finally, on top of the coating there exists a zone characterized by a lot of

pores and relative large, prismatic grains which seem to be only loosely attached to the underlying coating area. As the observed recession effects were triggered by the reducing atmosphere, a gas-phase reaction of Y_2SiO_5 with CO is obvious and should be reflected in the newly formed phases. An EDS line scan was measured across the recession zone as indicated by the dotted arrow in fig. 16. In fig. 16 the normalized molar cation content of Si and Y is plotted versus the respective EDS spots. The EDS data indicate that the large prismatic crystals on top of the coating are essentially pure Y_2O_3. The slightly darker, less porous zone consists of a 50:50 Y-silicate, obviously $Y_2Si_2O_7$. The third newly formed zone with significant pore coalescence has a Y:Si ratio of approximately 60:40 which would match best the Y-oxyapatite phase $Y_{4.67}(SiO_4)_3O$. The phase sequence finalizes with stoichiometric Y_2SiO_5 (Y:Si = 67:33). The phase sequence raises the question whether only volatilization of species or additional diffusion processes have occurred. Considering Si as being volatilized according to $SiO_2(s) + CO(g) \rightarrow SiO(g) + CO_2(g)$ the formation of the Y-rich outer layer is plausible. On the other hand, there is a decreasing Si content in the following phase sequence $Y_2Si_2O_7$ - $Y_{4.67}(SiO_4)_3O$ - Y_2SiO_5, i.e. an enrichment of Si towards the outside, which apparently is a conflicting behavior. On the contrary, if Y would be considered volatile its outward depletion from Y_2SiO_5 over $Y_{4.67}(SiO_4)_3O$ to Y_2SiO_7 is plausible, but the presence of the Y-rich outer layer would be hard to rationalize. Therefore, one may conclude that Si is essentially the mobile species, however, does not completely evaporate but also diffuses inward and causes the formation of Si-enriched phases such as $Y_2Si_2O_7$ and $Y_{4.67}(SiO_4)_3O$. In any case Y_2SiO_5 coatings are prone to recession in reducing atmosphere, consequently respective applications are considered critical. With respect to coating adhesion, results suggest that it may be hard to obtain strongly adhering Y_2SiO_5 coatings on “perfect”, i.e. essentially pure SiC surfaces. This is simply due the fact that chemical

bonding between predominantly ionically bonded crystals (such as oxides) and covalently bonded crystals (such as non-oxides) is generally limited. A thin, glassy SiO_2 layer generated by SiC oxidation significantly improves Y_2SiO_5 adhesion on SiC substrates. Most of the SiO_2 does react with Y_2SiO_5 to a $Y_2Si_2O_7$ interlayer. Interestingly, analogous $RE_2Si_2O_7$ (RE=rare earth) interlayers between have been proposed as part of multilayer environmental barrier coatings, thereby separating the bond-coat and the Y_2SiO_5 protective layer.[25] Such kind of interlayer is generated in the present system by accident. The major drawback, however, is the limited high-temperature stability of residual amorphous SiO_2 which frequently crystallizes to β-cristobalite in the 1273-1473 K range. Upon cooling to room temperature cristobalite goes through a displacive phase transformation with high associated volume change and therefore is prone to cracking and spallation, in particular in thermocyclic operation. Moreover, free SiO_2 is evidently prone to recession in combustion atmospheres; consequently long term durability is questionable.

4. Conclusions and Outlook

(1) The results prove the feasibility of magnetron sputtering of Y_2SiO_5 coatings for ceramic matrix composites. Drawbacks are low deposition rates and limited substrate dimensions. The current coating porosity of ~25 vol% may be reduced by additional substrate heating providing better surface diffusion.

(2) Although the as-deposited Y_2SiO_5 coatings are amorphous and homogeneous, a direct formation of the HT-polymorph X_2-Y_2SiO_5 was not observed, instead metastable apatite-type $Y_{4.67}(SiO_4)_3O$ and X_1-Y_2SiO_5 are forming below 1473 K.

(3) Consistent with subsolidus phase relations in the system Y_2O_3-Al_2O_3-SiO_2 the Y_2SiO_5/Al_2O_3 interface is thermodynamically unstable and decomposes to a well-

bound $Y_2Si_2O_7$/YAG double layer. On the other hand, this occurs only at temperatures exceeding envisaged all-oxide CMC operation conditions. Nonetheless, interface stability may be improved by introducing of an additional Y-aluminate interphase.

(4) Annealing in different atmospheres provided evidence that good adhesion of Y_2SiO_5 coatings on non-oxide CMC such as SiC-coated C/SiC is mainly due to amorphous SiO_2 deriving from SiC-oxidation. SiO_2 and Y_2SiO_5 form an additional $Y_2Si_2O_7$ interphase. However, the residual amorphous SiO_2 interphase is considered critical due to cristobalite formation and related danger of spallation.

References

[1] J. D. Webster, M. E. Westwood, F. A. Hayes, R. J. Day, R. Taylor , A. Durán, M. Aparicio, K. Rebstock, W. D. Vogel, J. Eur. Ceram. Soc. 18 (1998) 2345-50

[2] M. Aparicio, A. Durán, J. Am. Ceram. Soc. 83 (2000)1351–55

[3] H. J. Seifert, S. Wagner, O. Fabrichnaya, H.L. Lukas, F. Aldinger, T. Ullmann, M.Schmücker, H. Schneider, J. Am. Ceram. Soc. 88 (2005) 424-30

[4] K. N. Lee, D. S. Fox, N. P. Bansal, J. Eur. Ceram. Soc. 25 (2005) 1705–15

[5] M. Fritsch, H. Klemm, M. Herrmann, B. Schenk, J. Eur. Ceram. Soc. 26 (2006) 3557-65.

[6] M. Fritsch, H. Klemm, in: D. Zhu (ed.) Ceram. Eng. & Sci. Proc. 2006;27.3 (2007) Wiley, Hoboken, NJ

[7] H. M. O'Bryan, P. K. Gallagher, G. W. Berkstresser, J. Am. Ceram. Soc. 71 (1988) C42-C43

[8] Y. Ogura, M. Kondo, T. Morimoto, Y. Takeda, A. Notomi, J. Japan Inst. of Metals 63 (1999) 1295-1303

[9] J. W. Nowok, J. P. Kay, R. J. Kulas, J. Mater. Res. 16 (2001) 2251-55

[10] K. Fukuda and H. Matsubara, J. Mater. Res. 18 (2003) 1715-22

[11] Z. Sun, M. Li, Y. Zhou, J. Eur. Ceram. Soc. 29 (2009) 551–57

[12] Y. Ogura, M. Kondo, T. Morimoto, A. Notomi, T. Sekigawa, Mat. Trans. 42 (2001)

[13] B.Liu, J. Wang, F. Li, J. Wang, Y. Zhou, J. Am. Ceram. Soc. 95 (2012) 1093-99

[14] J.-F. Huang, X.-R. Zeng, H.-J. Li, X. Xiong, Y.-W. Fu, M. Huang, J. Mat. Sci. Lett. 39 (2004) 7383 – 85

[15] C. Argirusis, T. Damjanović, M. Stojanović, G. Borchardt, Mat. Sci. For. 494 (2005) 451-56

[16] C. Argirusis, T. Damjanovic, G. Borchardt, J. Eur. Ceram. Soc. 27 (2007) 1303–6

[17] J. Liu, L. Zhang, F. Hu, J. Yang, L. Cheng, Y. Wang, J. Eur. Ceram. Soc. 33 (2013) 433–39

[18] A. Ito, J. Endo, T. Kimura, T. Goto, Surf. Coat. Techn. 204 (2010) 3846–50

[19] A. Ito, J. Endo, T. Kimura, T. Goto, Mat. Chem. Phys. 125 (2011) 242–46

[20] O. Yamaguchi, K. Matui, K. Shimizu, Ceram. Int. 11 (1985), 107-108

[21] A. S. Gandhi, C. G. Levi, J. Mater. Res. 20 (2005), 1017-1025

[22] U. Kolitsch, H. J. Seifert, T. Ludwig, F. Aldinger, J. Mater. Res. 14 (1999) 447-55

[23] O. Fabrichnaya, H. J.Seifert , R. Weiland, T. Ludwig, F. Aldinger, A. Navrotsky, Z. Metallkunde 92 (2001), 1083-97

[24] Z. Sun, J. Wang, M. Li, Y. Zhou, J. Eur. Ceram. Soc. 28 (2008) 2895–2901

[25] P. J. Meschter, C. A. Johnson, K. L. Luthra, R. Sarrafi-Nour, U.S. Patent Application 2009/0250153 A1 (2009)

Figure captions

Fig. 1: Microstructure of as-sputtered, X-ray amorphous Y_2SiO_5 on a porous Al_2O_3 CMC substrate. The coating surface exhibits typical cauliflower morphology. The cross section reveals tilted columnar features originating from a 2 μm thick root zone.

Fig. 2: An EDS scan through the coating thickness confirms the accuracy and homogeneity of the sputter process.

Fig. 3: Phase formation upon annealing amorphous Y_2SiO_5 coatings in air. At 1273K crystallization products are Apatite-type $Y_{4.66}(SiO_4)_3O$ and low-temperature polymorph X_1-Y_2SiO_5. X_2-Y_2SiO_5 appears at 1373 K predominantly at the expense of apatite. At 1473 K only the high-temperature polymorph X_2-Y_2SiO_5 exists.

Fig. 4: Microstructure of Y_2SiO_5 coating upon 1h annealing at 1273 K. The coating surface still exhibits cauliflower morphology but small nanoscaled crystals appear. The cross section shows columnar grains separated by aligned pores.

Fig. 5: Upon 1h annealing at 1373 K the coating surface shows grain growth whereas the cross sectional view still is characterized by aligned pores. However, grain elongation is less pronounced.

Fig. 6: A substantially evolving microstructure is observed upon 1 h annealing at 1473 K. The coating surface shows newly formed up to 2 mm grains. The cross section reveals grain growth, significant pores coalescence and disappearance of alignment.

Fig. 7: Progressive grain growth and pore coalescence as observed upon 1 h annealing at 1573 K. At the coating/substrate interface a continuous, brightly contrasted layer is developing (white arrows). The close-up (inset) discloses that two new phases form a double layer.

Fig. 8: Progressive grain growth and pore coalescence as observed upon 1 h annealing at 1673 K. The double-layer at interface has grown to about 5 μm and clearly consists of two different crystalline species.

Fig. 9: EDS scan revealing the chemical nature of the newly formed double layer at the Y_2SiO_5/Al_2O_3 interface: A layer with nearly $Y_2Si_2O_7$ stoichiometry co-exists with Y_2SiO_5. Next towards the Al_2O_3 substrate follows a Y-aluminate which can be assigned to a YAG-type solid solution (YAG: $Y_3Al_5O_{12}$).

Fig. 10: Isothermal section through the ternary Y_2O_3-Al_2O_3-SiO_2 phase diagram and calculated subsolidus phase relations at 1673 K (adapted after Kolitsch et al. [22]; Fabrichnaya et al.[23]) Y_2SiO_5 and Al_2O_3 do not co-exist at 1673 K. The dot marker located close to the join $Y_2Si_2O_7$ - $Y_3Al_5O_{12}$ (thick line) represents the Y_2SiO_5/Al_2O_3 interface composition; hence formation of $Y_2Si_2O_7$ and $Y_3Al_5O_{12}$ is expected.

Fig. 11: Microstructure of as-sputtered, X-ray amorphous Y_2SiO_5 on a CVD-SiC coated C/SiC CMC substrate. Compared to the oxide substrate (fig.1) the cauliflower surface morphology is less regular. The cross section reveals good conformity, less pronounced columnar growth, and a similar root zone.

Fig. 12: Evolution of the Y_2SiO_5/SiC interface upon 1 h annealing in N_2 at 1273, 1373 and 1473 K, respectively. Note partial coating spallation at 1273 K and full spallation at 1373 K. At 1473 K a thin porous layer partially bridges the gap between Y_2SiO_5 and SiC. Primarily vertical cracks are evolving in Y_2SiO_5.

Fig. 13: Close-up of the Y_2SiO_5/SiC interface upon 1 h annealing in N_2 at 1473K. The porous interlayer is identified by EDS as $Y_2Si_2O_7$ which has formed from Y_2SiO_5 and amorphous SiO_2 derived from SiC-oxidation. Residual SiO_2 is occasionally still wetting the SiC surface.

Fig. 14: Y_2SiO_5/SiC interface upon 1 h annealing in air at 1473 K. Note improved coating adhesion due to formation of a quasi-continuous porous interphase (overview). The close-up shows newly formed $Y_2Si_2O_7$ bridging the gap between Y_2SiO_5 and SiC and continuous wetting of the SiC surface by SiO_2.

Fig. 15: Y_2SiO_5/SiC interface upon 1 h annealing in a reducing N_2/CO atmosphere at 1473 K. The coating shows massive blistering and exfoliation. A recession zone with a sequence of newly formed phases is formed at the gas-phase contact. The dotted arrow indicates the position of the EDS scan plotted in fig. 16.

Fig. 16: EDS scan of the recession zone (see inset and fig. 15) reveals an overlay with very high Y-content followed by two Y-silicates with increasing Y:Si ratio which can be assigned to $Y_2Si_2O_7$ and $Y_{4.66}(SiO_4)_3O$, respectively.

Figure 1

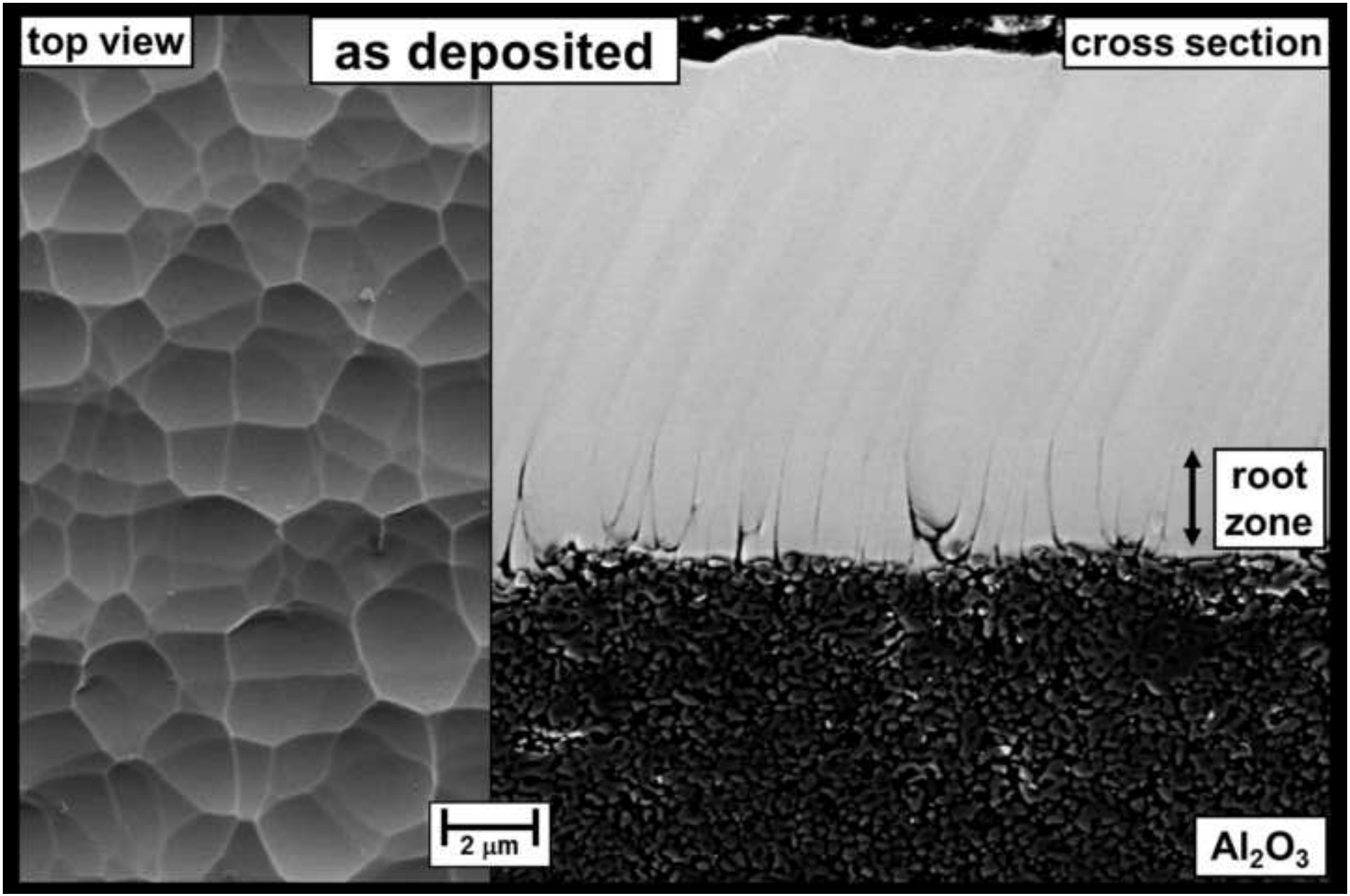

Figure 2

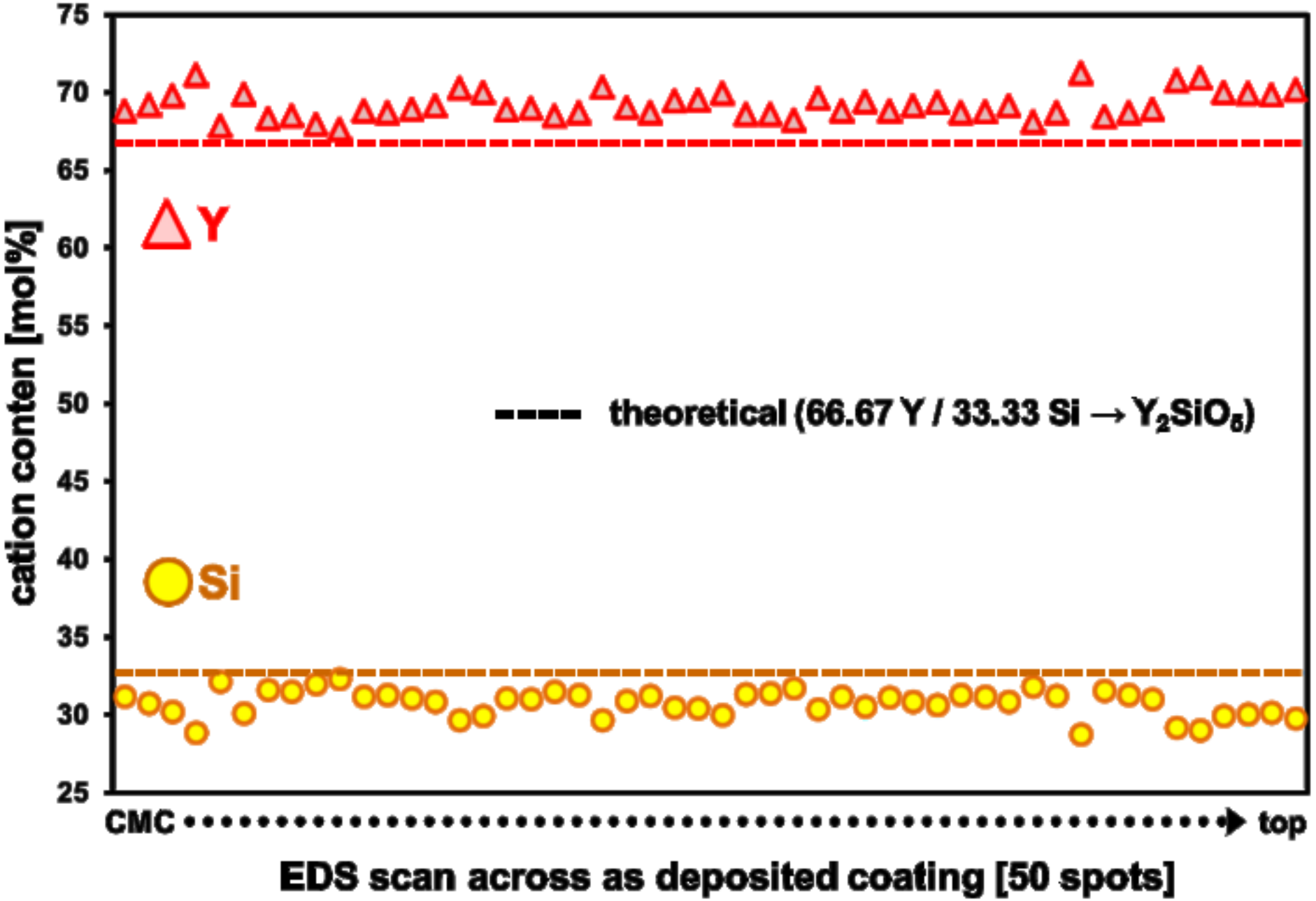
75
70
65
60
55
50
45
40
35
30
25
cation conten [mol%]
Y
Si
theoretical (66.67 Y / 33.33 Si → Y2SiO5)
CMC
top
EDS scan across as deposited coating [50 spots]

Figure 3

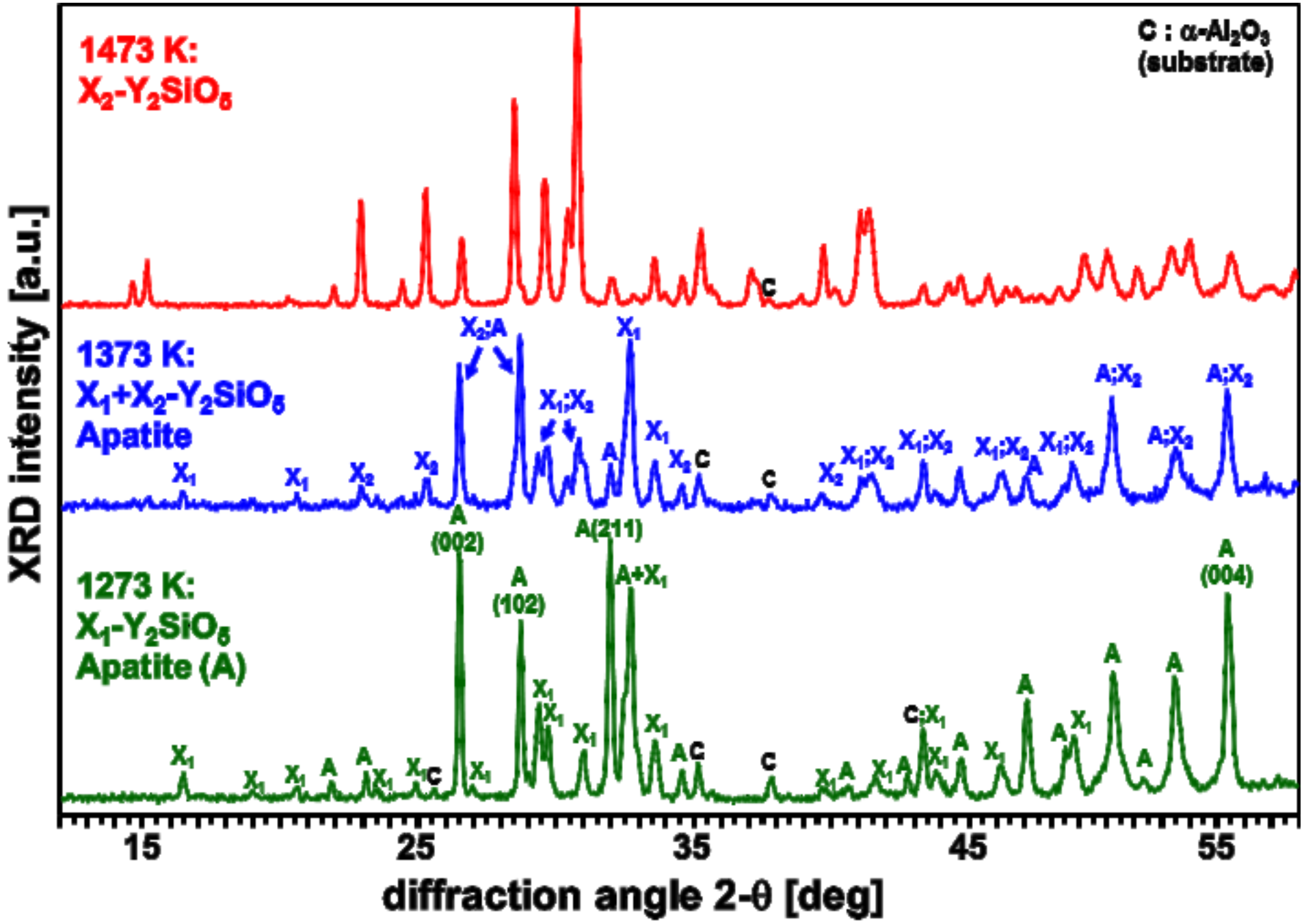
1473 K:
X2-Y2SiO5
C : α-Al2O3
(substrate)
1373 K:
X1+X2-Y2SiO5
Apatite
1273 K:
X1-Y2SiO5
Apatite (A)
XRD intensity [a.u.]
diffraction angle 2-θ [deg]
15
25
35
45
55
A (002)
A (102)
A(211)
A+X1
A (004)
X2:A
X1:X2
A:X2
C:X1

Figure 4

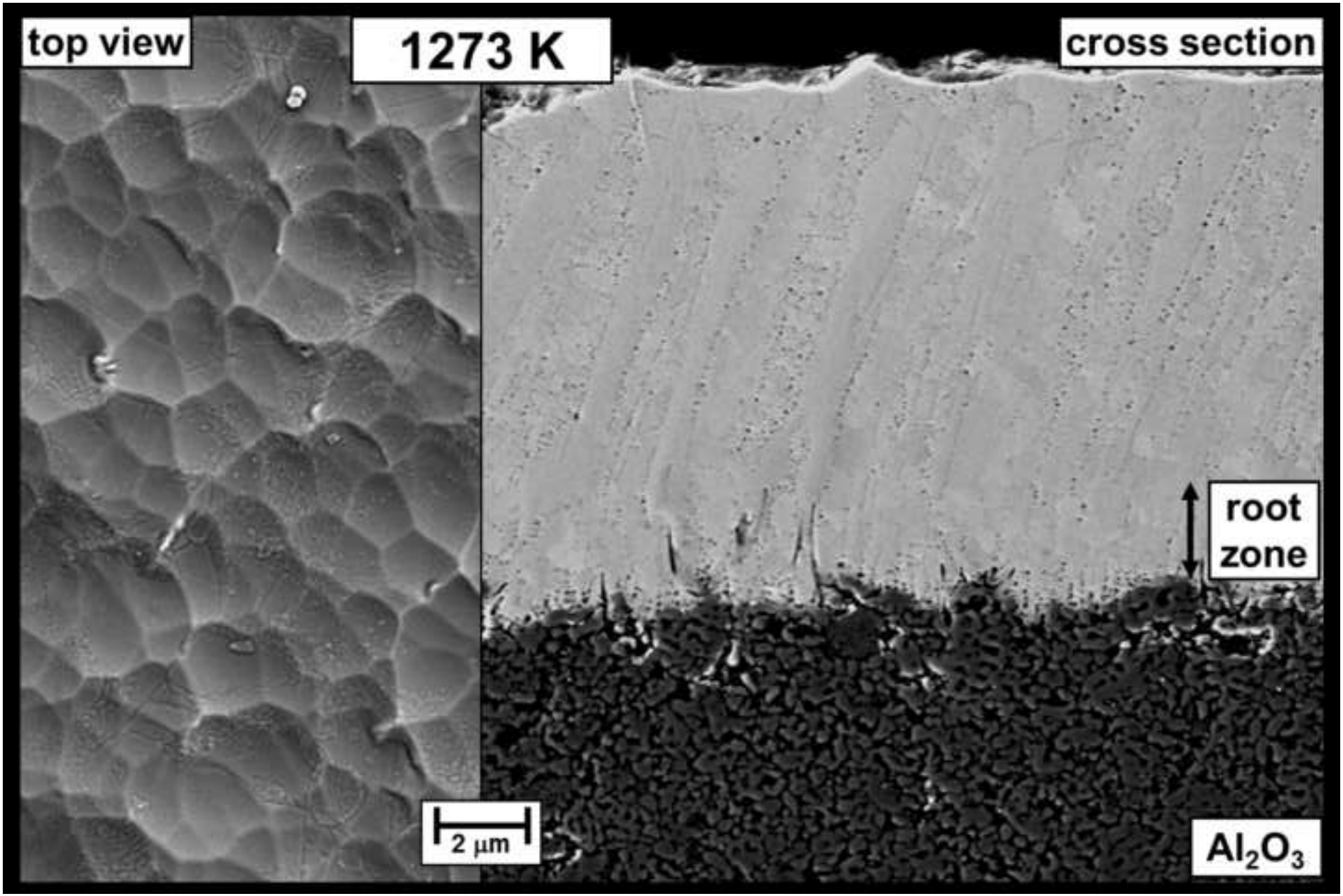

Figure 5

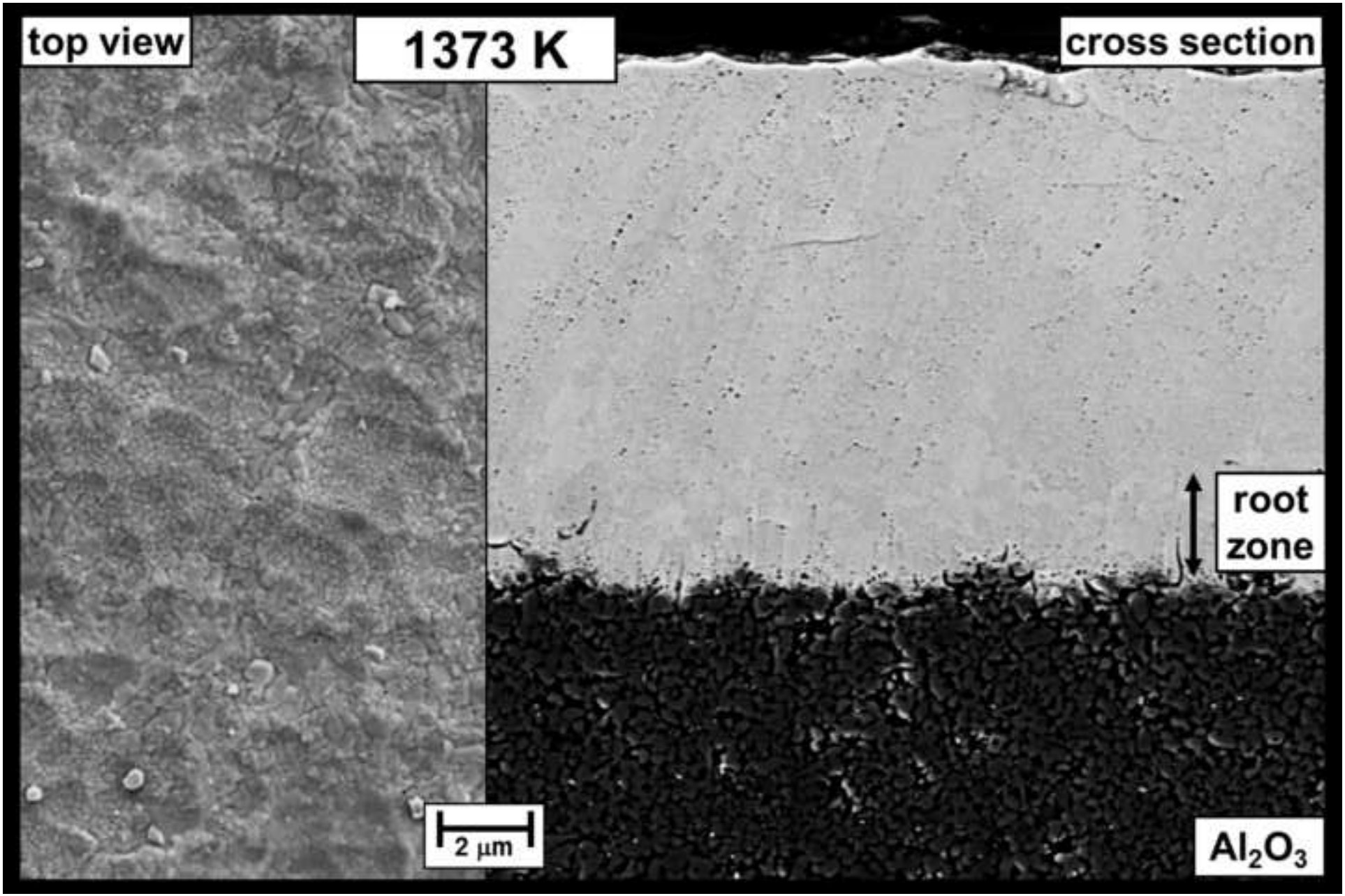

Figure 6

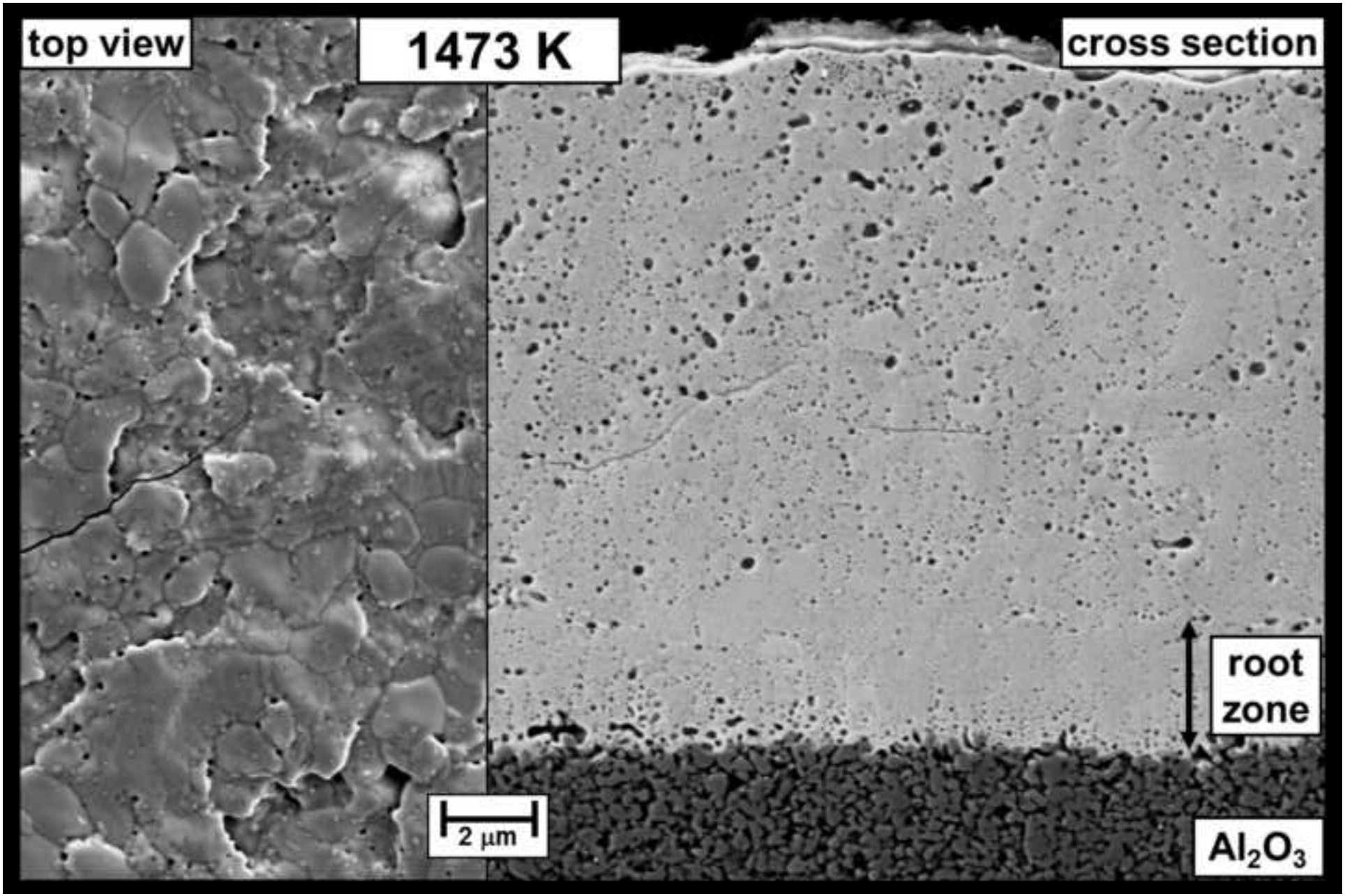

Figure 7

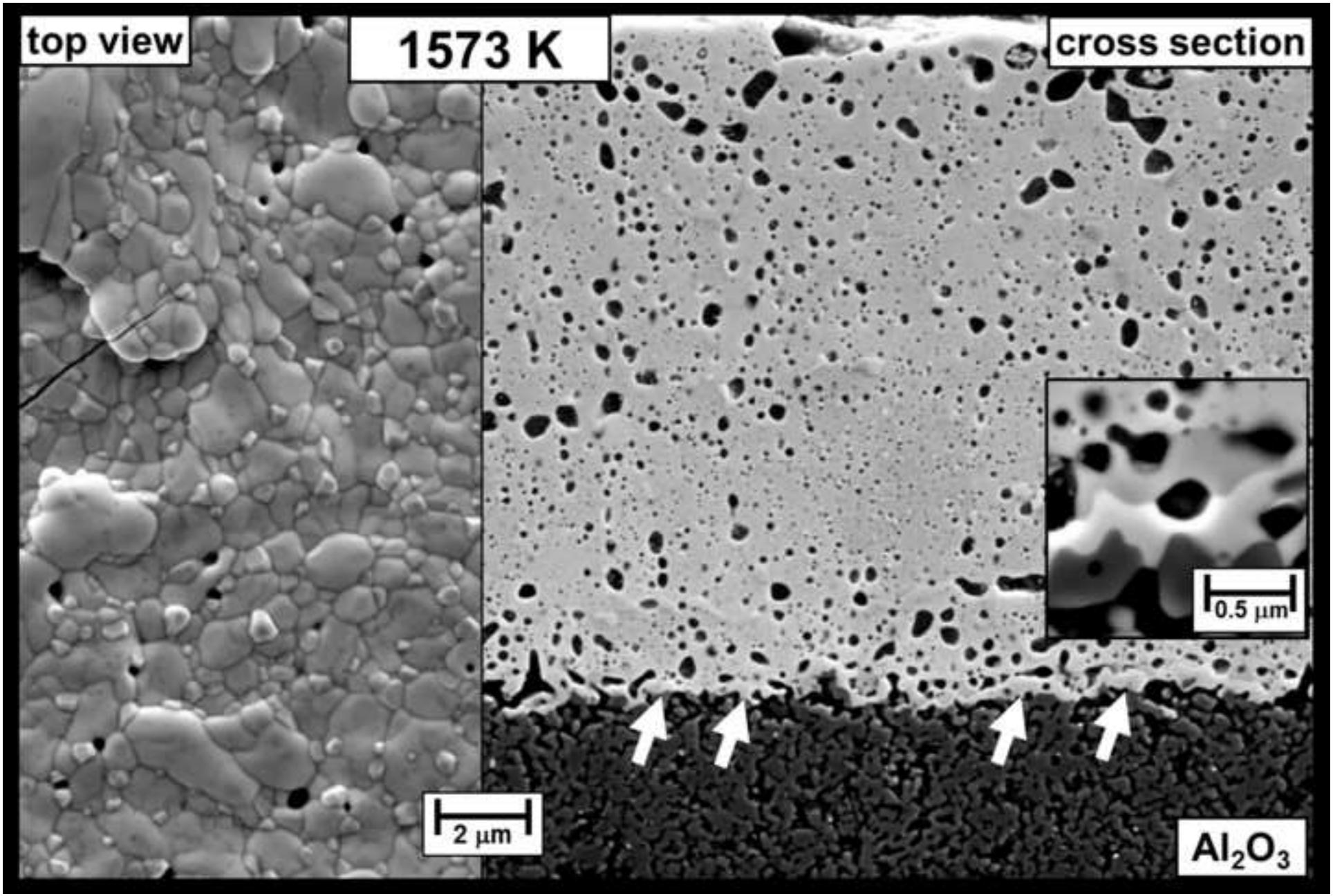

Figure 8

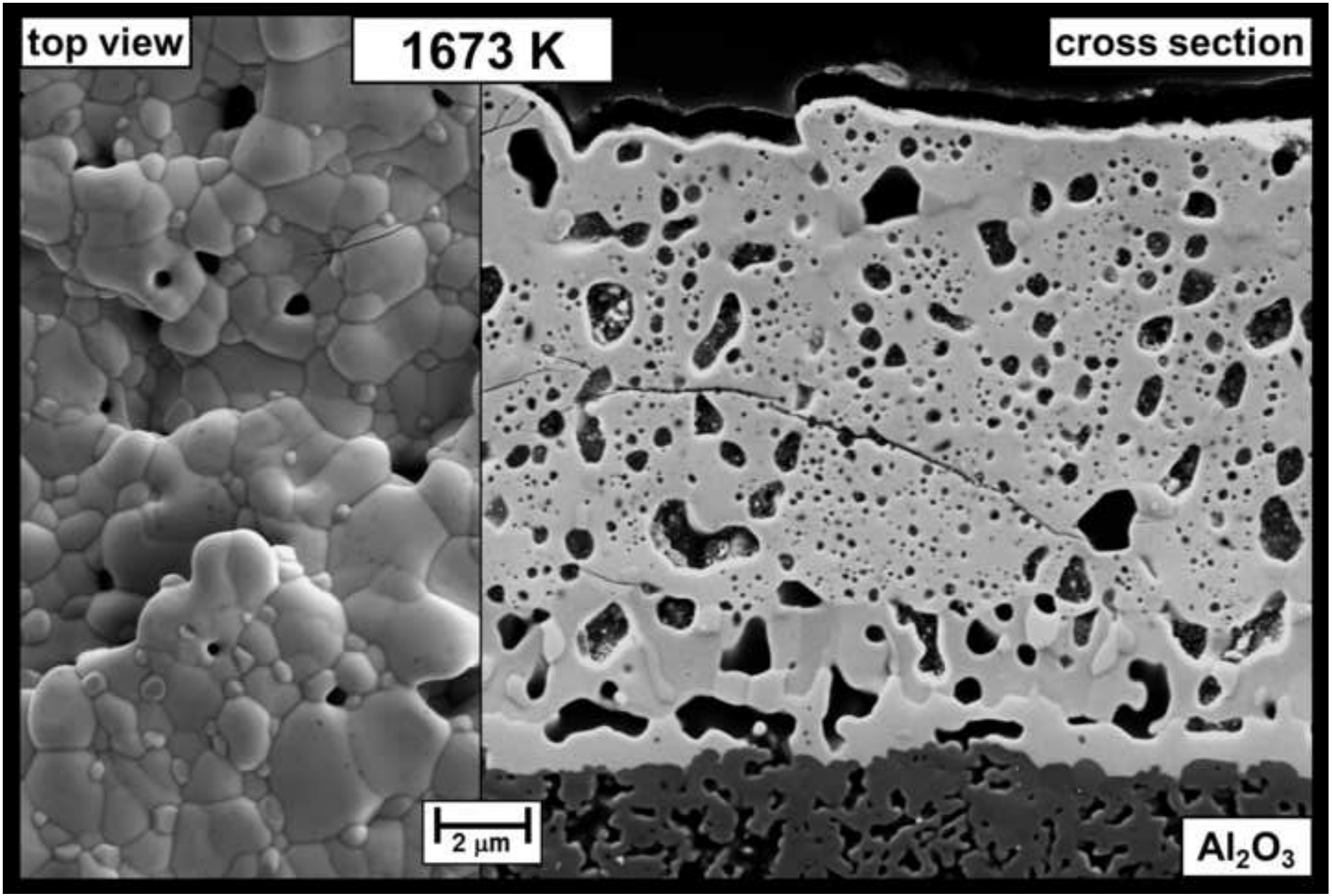

Figure 9

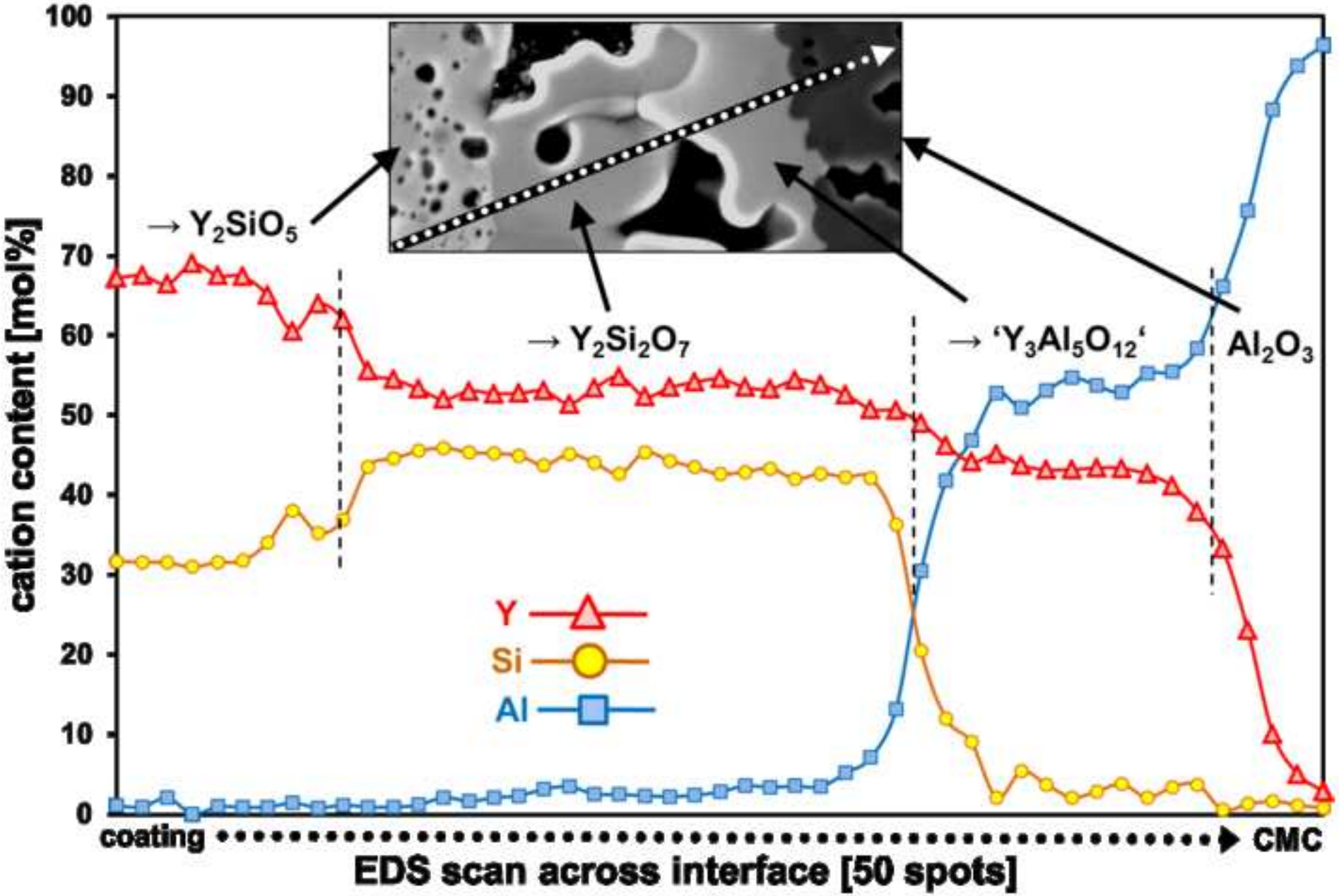
100
90
80
70
60
50
40
30
20
10
0
cation content [mol%]
→ Y2SiO5
→ Y2Si2O7
→ 'Y3Al5O12'
Al2O3
Y
Si
Al
coating
CMC
EDS scan across interface [50 spots]

Figure 10

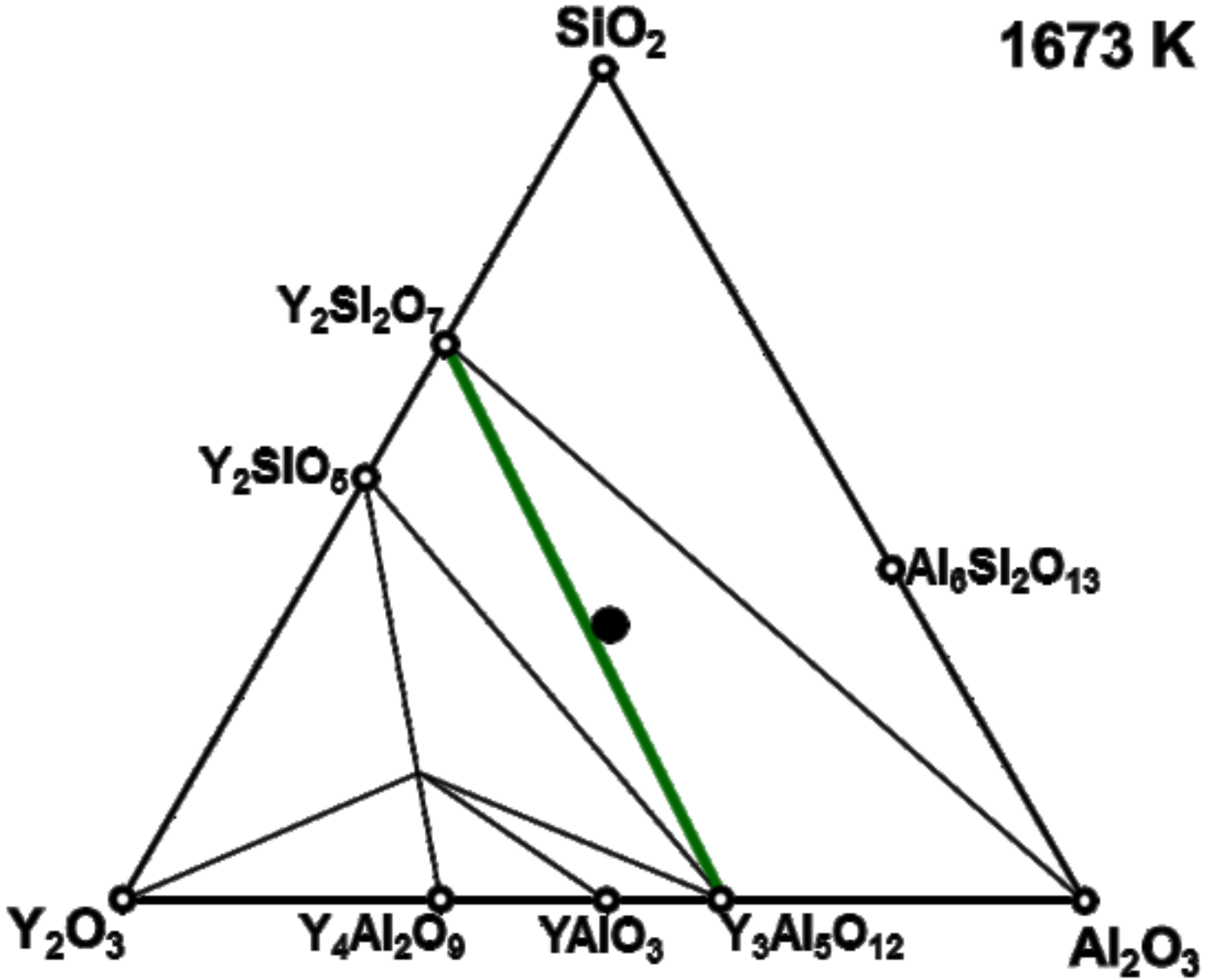

● $Y_2SiO_5 + Al_2O_3 \rightarrow Y_2O_3 \cdot Al_2O_3 \cdot SiO_2$

Figure 11

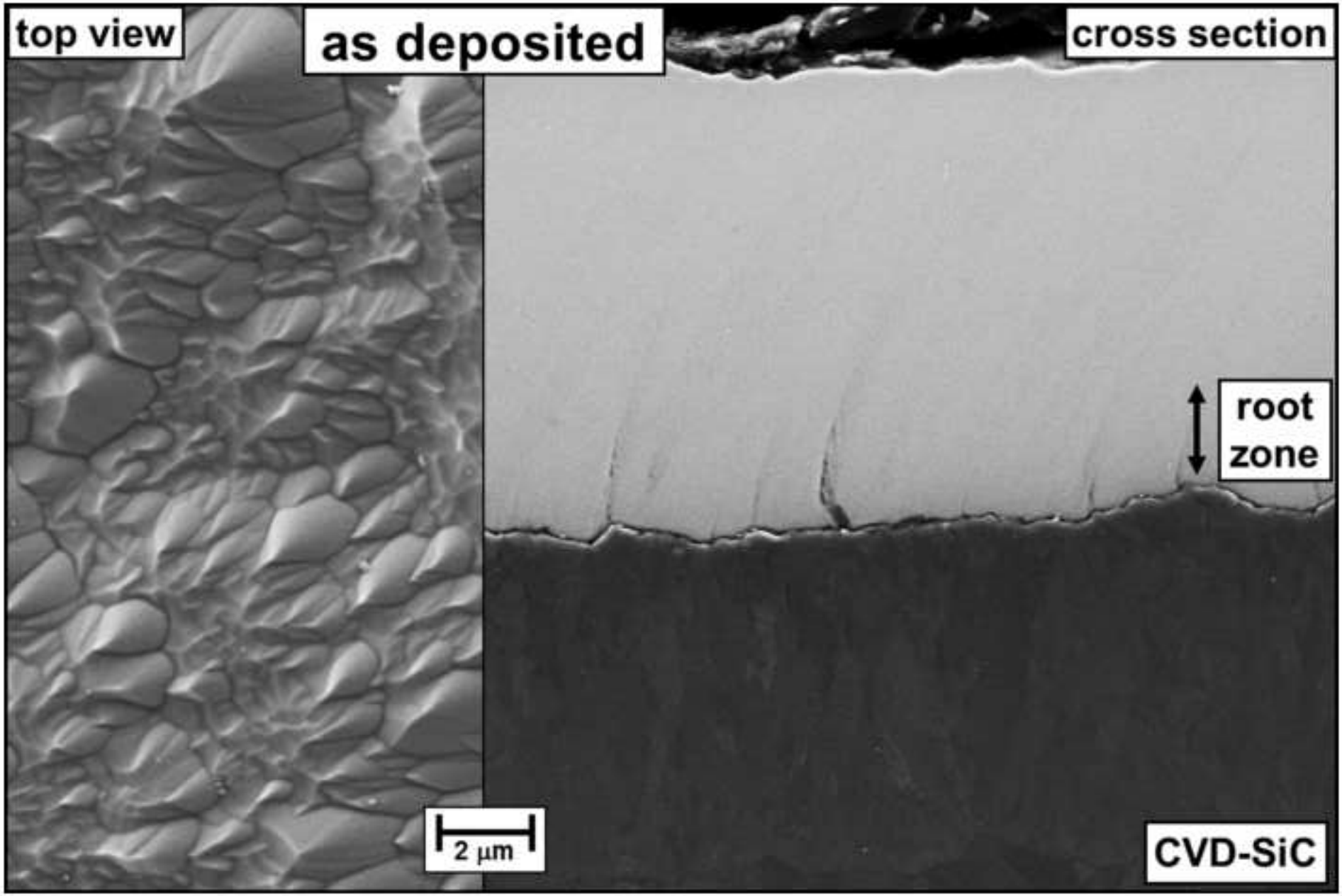

Figure 12

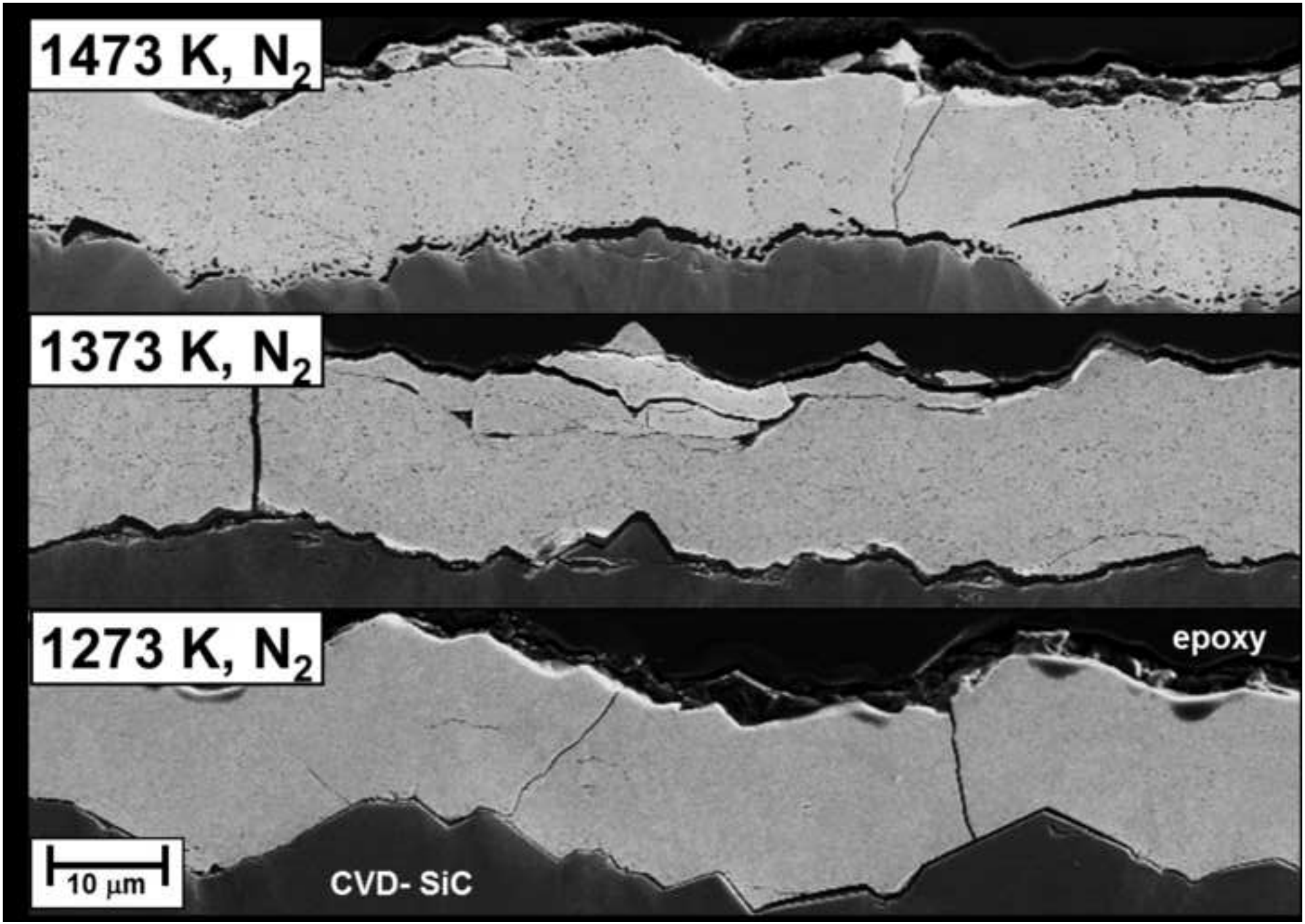

Figure 13

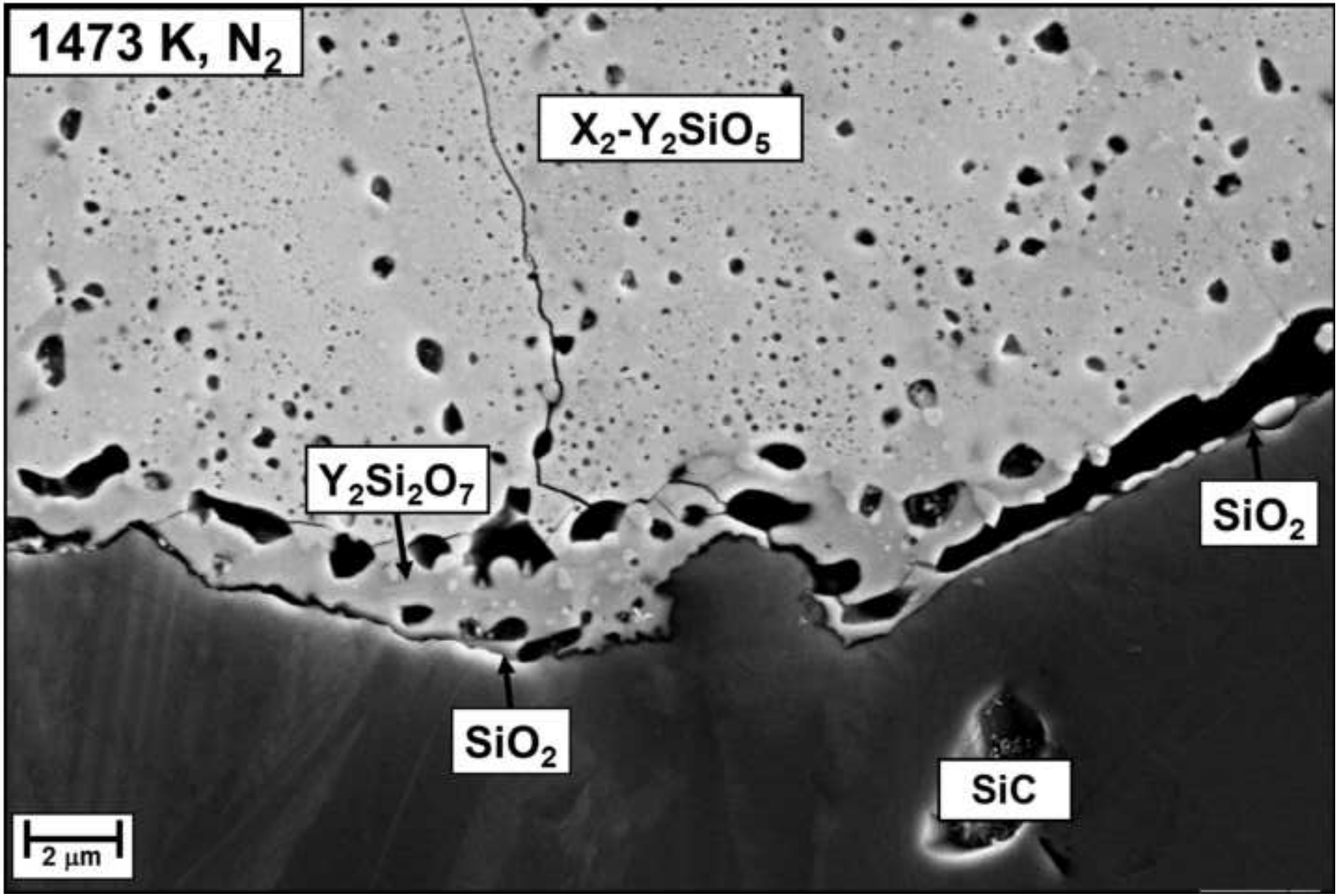

Figure 14

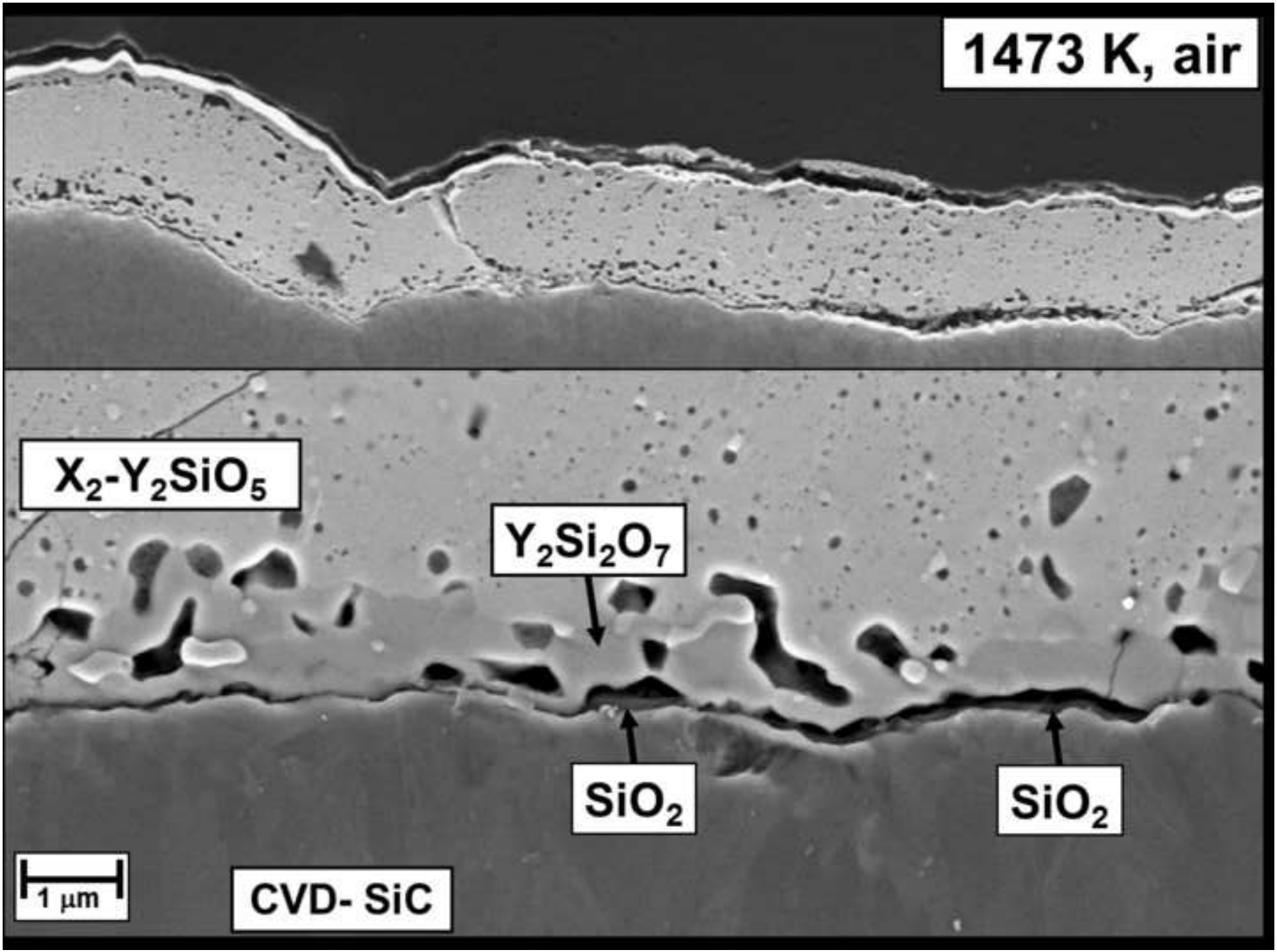

Figure 15

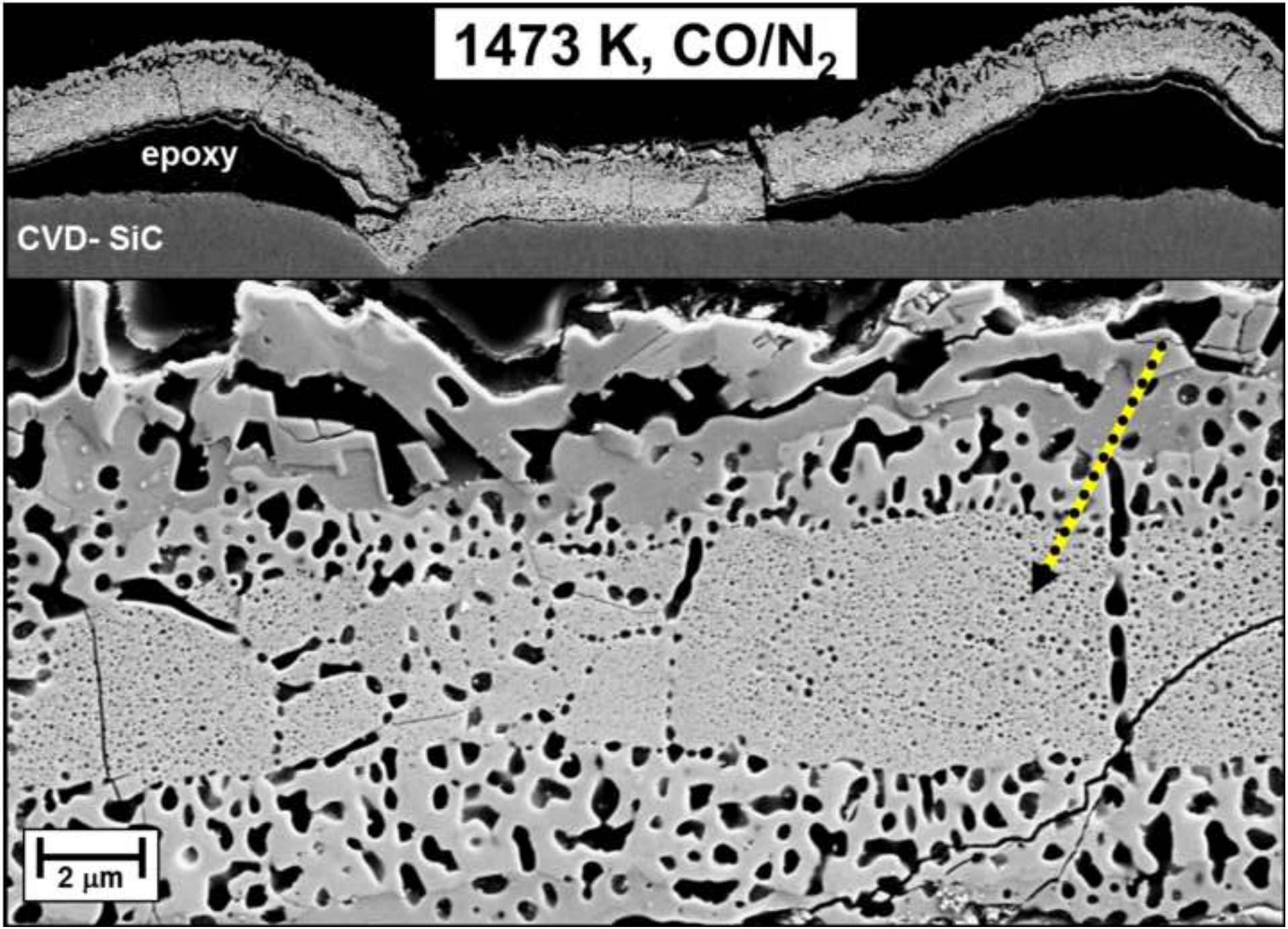

Figure 16

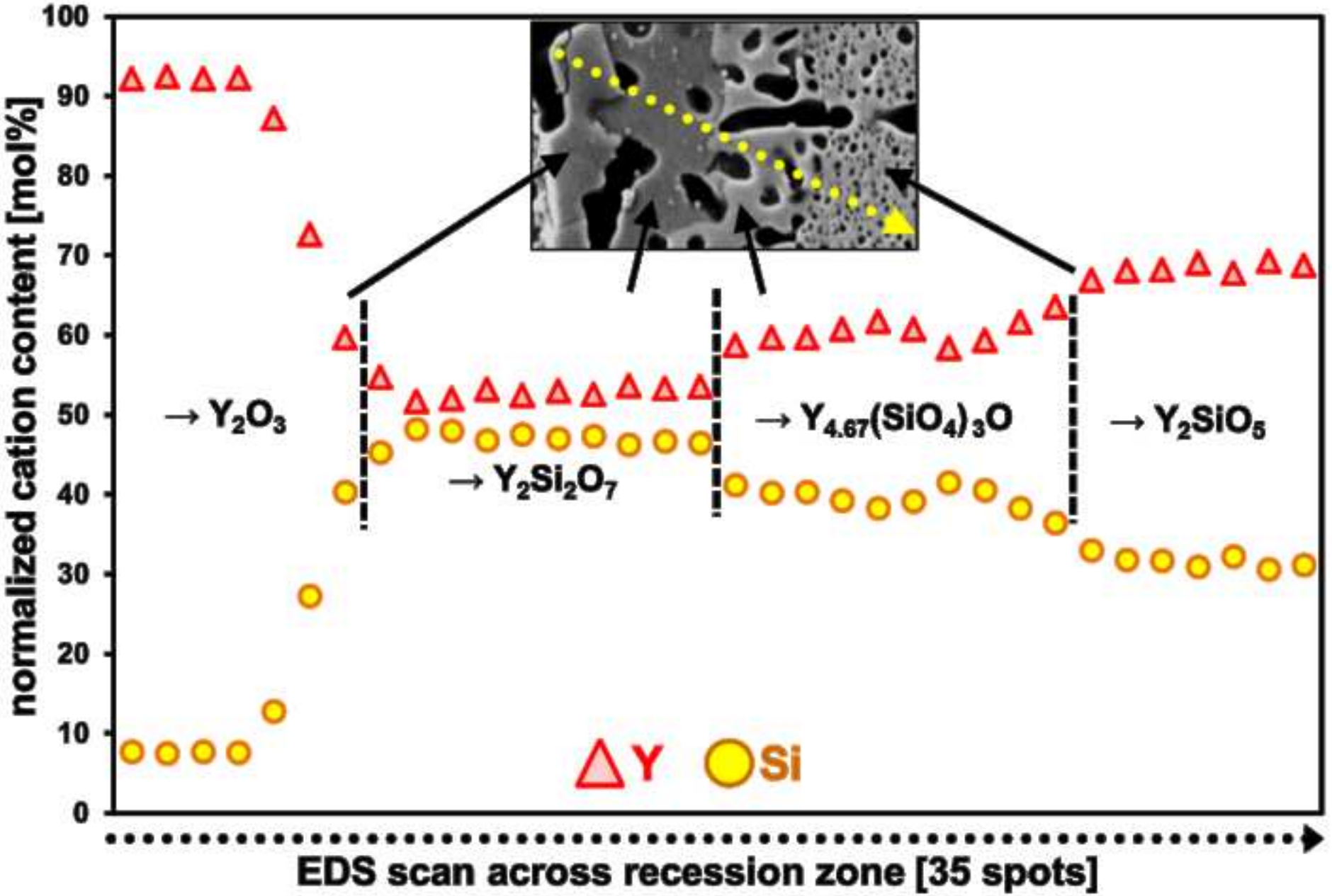
100
90
80
70
60
50
40
30
20
10
0
normalized cation content [mol%]
→ Y2O3
→ Y2Si2O7
→ Y4.67(SiO4)3O
→ Y2SiO5
Y
Si
EDS scan across recession zone [35 spots]